

Aerodynamic ground effect in fruitfly sized insect takeoff

Dmitry Kolomenskiy^{1,6†}, Masateru Maeda², Thomas Engels^{3,4},
 Hao Liu^{1,5}, Kai Schneider³ and Jean-Christophe Nave⁶

¹Graduate School of Engineering, Chiba University, 1-33 Yayoi-cho,
 Inage-ku, Chiba-shi, Chiba 263-8522, Japan

²Department of Biology, Lund University, Ecology Building, SE-223
 62 Lund, Sweden

³M2P2-CNRS, Université d'Aix-Marseille, 39, rue Frédéric
 Joliot-Curie, 13453 Marseille Cedex 13, France

⁴Institut für Strömungsmechanik und Technische Akustik (ISTA),
 TU Berlin, Müller-Breslau-Str. 8, 10623 Berlin, Germany

⁵Shanghai-Jiao Tong University and Chiba University International
 Cooperative Research Center, 800 Dongchuan Road, Minhang
 District, Shanghai, China

⁶Department of Mathematics and Statistics, McGill University, 805
 Sherbrooke W., Montreal, QC, H3A 0B9, Canada

E-mail: dkolom@gmail.com

Abstract. Flapping-wing takeoff is studied using numerical modelling, considering the voluntary takeoff of a fruitfly as reference. The parameters of the model are then varied to explore the possible effects of interaction between the flapping-wing model and the ground plane. The numerical method is based on a three-dimensional Navier–Stokes solver and a simple flight dynamics solver that accounts for the body weight, inertia, and the leg thrust. Forces, power and displacements are compared for takeoffs with and without ground effect. Natural voluntary takeoff of a fruitfly, modified takeoffs and hovering are analyzed. The results show that the ground effect during the natural voluntary takeoff is negligible. In the modified takeoffs, the ground effect does not produce any significant increase of the vertical force neither. Moreover, the vertical force even drops in most of the cases considered. There is a consistent increase of the horizontal force, and a decrease of the aerodynamic power, if the rate of climb is sufficiently small.

† Corresponding author: dkolom@gmail.com

1. Introduction

The aerodynamic forces of an air vehicle or an animal may be affected by the ground proximity. This phenomenon, known as the ground effect, has been extensively studied for aircraft [12] and rotorcraft [16]. Although the effect varies depending on many design parameters, the general trend is an increase in lift and pitching moment, and a decrease in drag. The effect decays as the distance from the ground increases, and vanishes at a distance larger than, but comparable with, the size of the vehicle.

Rayner [21] proposed a fixed wing lifting line theory for forward flight of birds, bats and insects. His analysis suggested that flight in ground effect provides performance improvements, if the flight speed is not too low. However, this theory could not be applied to hovering or slow forward flight at very low height, since it neglected flapping motion. Normal hovering in ground effect was considered by Gao and Lu [9]. They carried out two-dimensional numerical simulations of hovering and identified three regimes: force enhancement, force reduction, and force recovery, depending on the distance from the ground. Liu *et al.* [17] considered clap-and-fling near the ground and found force enhancement at all distances. A three-dimensional numerical simulation of fruitfly hovering was carried out by Maeda and Liu [19]. An increase in lift and a reduction in power was found. A significant vertical force was generated on the insect's body due to the 'fountain effect'. Energetic savings have also been reported for a hummingbird hovering in ground effect [13].

Several studies considered pitching-plunging foils near a solid wall or a free surface [24, 20, 26]. This configuration is relevant to fish swimming as well as forward flapping flight. The ground effect mainly consists in enhanced propulsive force. However, it also generates a non-zero vertical force due to asymmetry.

The main motivation for this study comes from the fact that the ground proximity is natural for takeoff and landing. These manoeuvres, unlike hovering or forward flight, are characterized by gradual change of distance to the ground. The 'dynamic' ground effect in these circumstances may be different from the 'static' effect at a constant distance [12]. This difference may be even larger for flapping wings than for fixed wings, because animals vary their wing kinematics during takeoff.

So far, the ground effect during takeoff has been assessed for very few insects only. It was found negligible for butterflies (*Pieris rapae* [2], *Papilio xuthus* [18]), a dronefly (*Eristalis tenax*) [5], and a fruitfly (*Drosophila virilis*) [4], but significant for a beetle (*Trypoxylus dichotomus*) [25]. The disparity can be attributed to significant differences in the size, morphology and kinematics of these insects.

In the present study, we consider a model having the morphology of a fruitfly, with variable wing kinematics and leg parameters. Our objective is to determine if the ground effect can be significant for this model, and which conditions can lead to it. We thus explore the parameter space of the model. First, for completeness, we revisit the voluntary takeoff of a fruitfly analyzed in [4]. The main difference with respect to [4] is the use of a flight dynamics solver. We then compare takeoffs with modified parameters

of the leg thrust model and wing kinematics. Finally, we consider hovering as a limiting case of very slow takeoff.

The paper is organized as follows. In section 2, we describe our computational approach and the takeoff parameters used in this study. The results are presented in section 3, first for a natural voluntary takeoff and then for modified takeoffs. Hovering flight is also considered, as a limiting case of very slow rate of climb. The main conclusions are summarized in section 4.

2. Models and methods

2.1. Morphology and kinematics

In this work, we consider a fruitfly having mass $m = 1.2$ mg and wing length $R = 2.83$ mm, which are the values reported in [4]. The body and wings are modelled as rigid solids. The wing contour used in this study is shown in figure 1(a). It is adapted from [4]. Its mean chord length is equal to $c = 0.85$ mm. The body is generated by sweeping a circular section of variable radius along a curvilinear centreline (an arc). It has approximately the same dimensions as in [4]. The side view of the body is shown in figure 1(c). To simplify the problem, we assume the bilateral symmetry. Therefore, the body orientation is fully defined by the pitch angle β between the body and the horizontal axis, see figure 1(b). The wing kinematics is described by the position angle ϕ , the feathering angle α and the elevation angle θ , measured with respect to the stroke plane, as shown in figure 1(d). It is convenient to refer to an ‘anatomical’ stroke plane η , i.e., to assume that the inclination of the stroke plane against the body axis is held at a constant angle for any motion of the body.

Case	Kinematics				Leg model				
	ϕ, α, θ	β	$\eta, {}^\circ$	$z_c(0)$, mm	L_ℓ , mm	K_ℓ^+ , N/m	$\phi_\ell^+, {}^\circ$	t_ℓ , ms	τ_ℓ , ms
Voluntary	fig.1e	fig.1e	62	1.08	1.24	0.165	84	4.2	1.3
Slow	fig.1e	fig.1e	62	1.08	1.24	0.041	84	4.2	1.3
Simplified	fig.7	46.3	32	3.11	1.24	0.0095...0.043	84	0	1.3
Hovering	fig.7	55	55	2.07	N/A	N/A	N/A	N/A	N/A

Table 1. Values of the leg thrust model parameters of the takeoffs considered in the present study.

Table 1 summarizes the parameters of the different cases considered in the present study. For the voluntary takeoff, the values of the body and wing angles are taken from one of the cases documented in [4]. However, the wing motion in [4] is not exactly symmetric. Therefore, the time series of ϕ , α and θ that we use for both wings correspond to the left wing data shown in [4]. Figure 1(e) presents the time evolution of the wing position angle $\phi(t)$, the feathering angle $\alpha(t)$, the elevation angle $\theta(t)$ and the body pitch angle $\beta(t)$, which are prescribed in our numerical simulations.

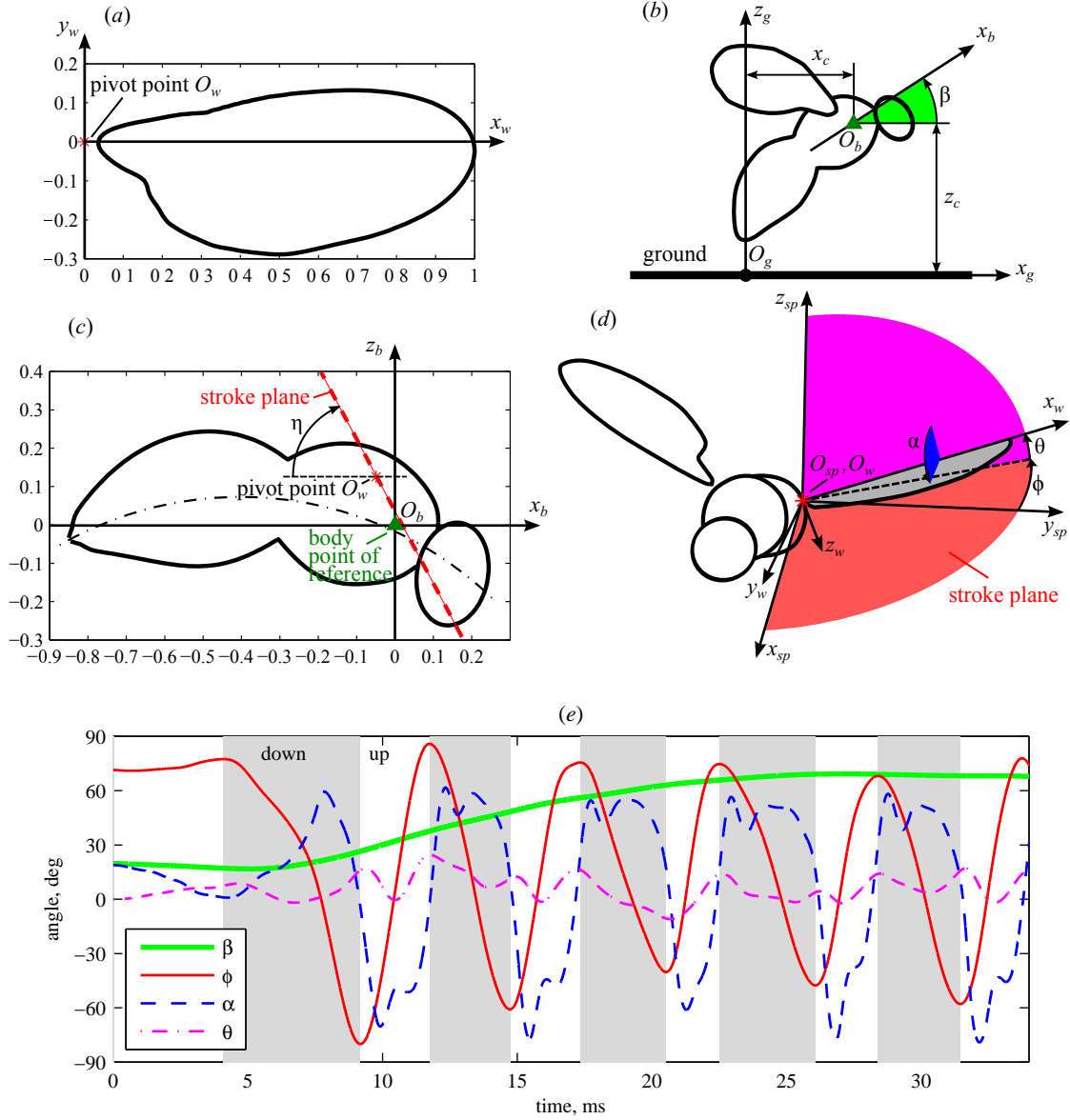


Figure 1. (a) Wing contour. Coordinates are normalized to the wing length R . (b) The insect's position with respect to the ground is described by the body point of reference coordinates (x_c, z_c) and the position angle β . (c) The body is generated by circular sections of variable radius, which changes depending on the position along the centre line (dash-dotted arc). The coordinates of the wing pivot points in the body frame of reference $O_b x_b y_b z_b$ are $(-0.07R, \pm 0.18R, 0.115R)$. (d) Definition of the wing's angles with respect to the stroke plane frame of reference $O_{sp} x_{sp} y_{sp} z_{sp}$. The origin O_{sp} is the wing pivot point. (e) Time evolution of the angular position of the body and of the wings during the voluntary takeoff.

Even though the wing motion is not exactly periodic, it is useful to introduce the wing beat frequency. When calculated using the average wing beat cycle period over the five cycles shown in figure 1(e), it is equal to $f = 169$ Hz. Similarly, the average wing beat amplitude is equal to 134° , and the average wing tip velocity is $U = 2.23$ m/s. The kinematic viscosity of air, equal to $\nu = 1.45 \cdot 10^{-5}$ m²/s yields the Reynolds number $Re = Uc/\nu = 131$. Note that U and Re do not account for the forward speed of the body.

Since the main focus of this study is the ground effect, it is important to ensure that the time evolution of the distance to the ground is consistent with the forces acting on the insect. For this reason, in our computations, unlike in [4], the position of the insect is dynamically computed as opposed to be prescribed. We compute the position of the body point of reference (x_c, z_c) , see figure 1(c), from Newton's 2nd Law,

$$m \frac{d^2 x_c}{dt^2} = F_{ax} + F_{\ell x}, \quad m \frac{d^2 z_c}{dt^2} = F_{az} + F_{\ell z} - mg, \quad (1)$$

where (F_{ax}, F_{az}) is the aerodynamic force, $(F_{\ell x}, F_{\ell z})$ is the leg thrust, subscripts x and z correspond, respectively, to the horizontal and vertical components, m is the insect's mass and g is the gravitational acceleration. Equations (1) are integrated using the adaptive second order Adams–Bashforth scheme [22], simultaneously with the incompressible Navier–Stokes equations. We defined the positive z direction to be upwards and the positive x direction to be forwards (see figure 1b).

2.2. Aerodynamics

The aerodynamic forces F_{ax} and F_{az} are obtained by solving the three-dimensional incompressible Navier–Stokes equations. The no-slip boundary condition at the body and wings surfaces is imposed using the volume penalization method [1], and the penalized equations are solved using a classical Fourier pseudo-spectral method. More details about the solver can be found in [14].

The computational domain in the present study is a rectangular box with sides L_x , L_y and L_z . It is discretized using a uniform Cartesian grid. Periodic boundary conditions are applied on all sides of the domain, as required by the Fourier discretization. Vorticity sponge boundary conditions are imposed at the left, right, rear and front sides of the domain, as explained in [7], in order to minimize the effect of the finite domain size. The ground surface is modelled as a solid layer at the bottom of the domain, which by periodicity also imposes the no-slip on the top of the fluid domain. We have carried out numerical experiments to ensure that, in the numerical simulations presented in this paper, the domain size is sufficiently large, i.e., its further increase does not change significantly the forces. The dimensions that we chose are also comparable with the size of the mineral oil tank used in the experiments with a mechanical model [6].

2.3. Leg thrust

The model of the leg thrust employed in the present study is a slight modification of the compression spring model proposed in [2]. We assume that takeoff begins from rest and starts at time $t = t_\ell$. The two components of the force are given by

$$F_{\ell x} = F_\ell \cot \phi_\ell, \quad F_{\ell z} = F_\ell. \quad (2)$$

The magnitude of the leg force is assumed to depend on the vertical component of the leg extension $\zeta = z_c(t) - z_c(t_\ell)$ only. The force is supposed to be distributed between the three pairs of legs such that its change with horizontal displacement can be neglected,

$$F_\ell = \begin{cases} (L_\ell - \zeta)K_\ell & \text{for } \zeta < L_\ell, \\ 0 & \text{for } \zeta \geq L_\ell, \end{cases} \quad (3)$$

where L_ℓ is the maximum leg extension length, i.e., the difference between the values of z_c when the legs are fully extended at takeoff and when the insect is at rest. When the legs are fully extended, $\zeta = L_\ell$, the legs lose contact with the ground and the force drops to zero. This length is estimated using video sequences in [4] to be equal to $L_\ell = 1.24$ mm. The rate K_ℓ varies in time: it increases from K_ℓ^- before takeoff to K_ℓ^+ after takeoff. The initial value $K_\ell^- = mg/L_\ell$ ensures that the insect is in equilibrium before takeoff, when the aerodynamic force is zero. The final value K_ℓ^+ is a parameter of the model that controls the maximum leg thrust. Its value can be estimated from the climb velocity at the beginning of takeoff, shown in, e.g., [4]. It may also be estimated from jumps of wingless flies [27, 3] for a closely related species, *D. melanogaster*. We assume the time evolution of K_ℓ of the form

$$K_\ell = \begin{cases} K_\ell^- & \text{for } t < t_\ell, \\ K_\ell^- + \frac{K_\ell^+ - K_\ell^-}{\tau_\ell}(t - t_\ell) & \text{for } t_\ell \leq t < t_\ell + \tau_\ell, \\ K_\ell^+ & \text{for } t \geq t_\ell + \tau_\ell. \end{cases} \quad (4)$$

The transition time τ_ℓ can be equal to zero, in which case the leg force increases impulsively at the beginning of takeoff. However, measurements of the leg force [27] suggest a gradual increase which can be accounted for by setting τ_ℓ to a value larger than zero. The direction ϕ_ℓ also changes in time. Before takeoff, when the insect is at rest, the force is applied only in the vertical direction, i.e., $\phi_\ell^- = 90^\circ$. During takeoff, the horizontal component is non-zero, in general. We assume a time evolution of the form

$$\phi_\ell = \begin{cases} \phi_\ell^- & \text{for } t < t_\ell, \\ \phi_\ell^- + \frac{\phi_\ell^+ - \phi_\ell^-}{\tau_\ell}(t - t_\ell) & \text{for } t_\ell \leq t < t_\ell + \tau_\ell, \\ \phi_\ell^+ & \text{for } t \geq t_\ell + \tau_\ell. \end{cases} \quad (5)$$

The values of the leg thrust model parameters used in our numerical simulations are given in table 1.

3. Results and discussion

The starting point for our study is the voluntary takeoff, as it is shown in section 3.1 (in agreement with [4]) that the ground effect is very small in that case. It is much smaller than during hovering (cf. [19]). We conjecture that this difference is due to the large takeoff vertical velocity, which is mainly the result of the leg thrust. To test this hypothesis, in section 3.2, we discuss a situation in which the legs produce less force and the insect takes off slower. The ground effect becomes significant. Surprisingly, the vertical force is decreased when the ground plane is present. In order to identify the mechanisms responsible for this adverse ground effect, we consider more different takeoff kinematics in section 3.3. Finally, in section 3.4, we find similar trends during the first wingbeats in hovering flights.

3.1. Voluntary takeoff

In this section, we consider voluntary takeoff of a fruitfly with the parameters as in the first line in table 1. This case shows some important general features of fruitfly takeoff such as the first wingbeat cycles beginning while the legs extend. Therefore it is likely that, despite some variability in voluntary takeoffs, the ground effect in general remains of the same order of magnitude in natural circumstances.

The computational domain size is equal to $L_x = L_y = 5R$, $L_z = 6R$, where R is the wing length. The number of grid points in each direction, respectively, is equal to $N_x = N_y = 640$ and $N_z = 768$. The penalization parameter is equal to $\varepsilon = 2.5 \cdot 10^{-4}$ (for details see, e.g., [7]).

The aerodynamic ground effect is evaluated by comparing two numerical simulations with two different values of the initial distance from the body point of reference to the ground: $z_c(0) = 0.38R$ and $2R$, which we denote ‘in ground effect’ (IGE) and ‘out of ground effect’ (OGE), respectively. The first case corresponds to a takeoff from a flat ground surface. In the second case, the leg model behaves as during takeoff from the ground, but the aerodynamic interaction between the insect and the ground is weak because of the large distance. This case may be interpreted as takeoff from a perch. With the distance equal to $2R$, the ground effect is negligible during hovering [18], therefore it is likely to be negligible during other types of manoeuvres.

Figure 2(f) shows the front and side view of the fruitfly model and of the wake, IGE, at 5 subsequent time instants. The vortices created by the wings and the body are identified as the volume of fluid enclosed by the iso-surfaces of the Q -criterion. At $t = 0$, the air is at rest. The insect body is almost horizontal. The wings are in a pre-takeoff position from which they begin the first downstroke after $t = 4.1$ ms. The time $t = 9.2$ ms corresponds to the first reversal from downstroke to upstroke. Because of the small body pitch angle β , the stroke plane is effectively vertical. In addition, the first downstroke is slow. Therefore, the vertical aerodynamic force is small, but the body lifts noticeably because of the leg thrust. The time $t = 12.8$ ms corresponds to the second upstroke. At this point, the distance from the body point of reference to the ground

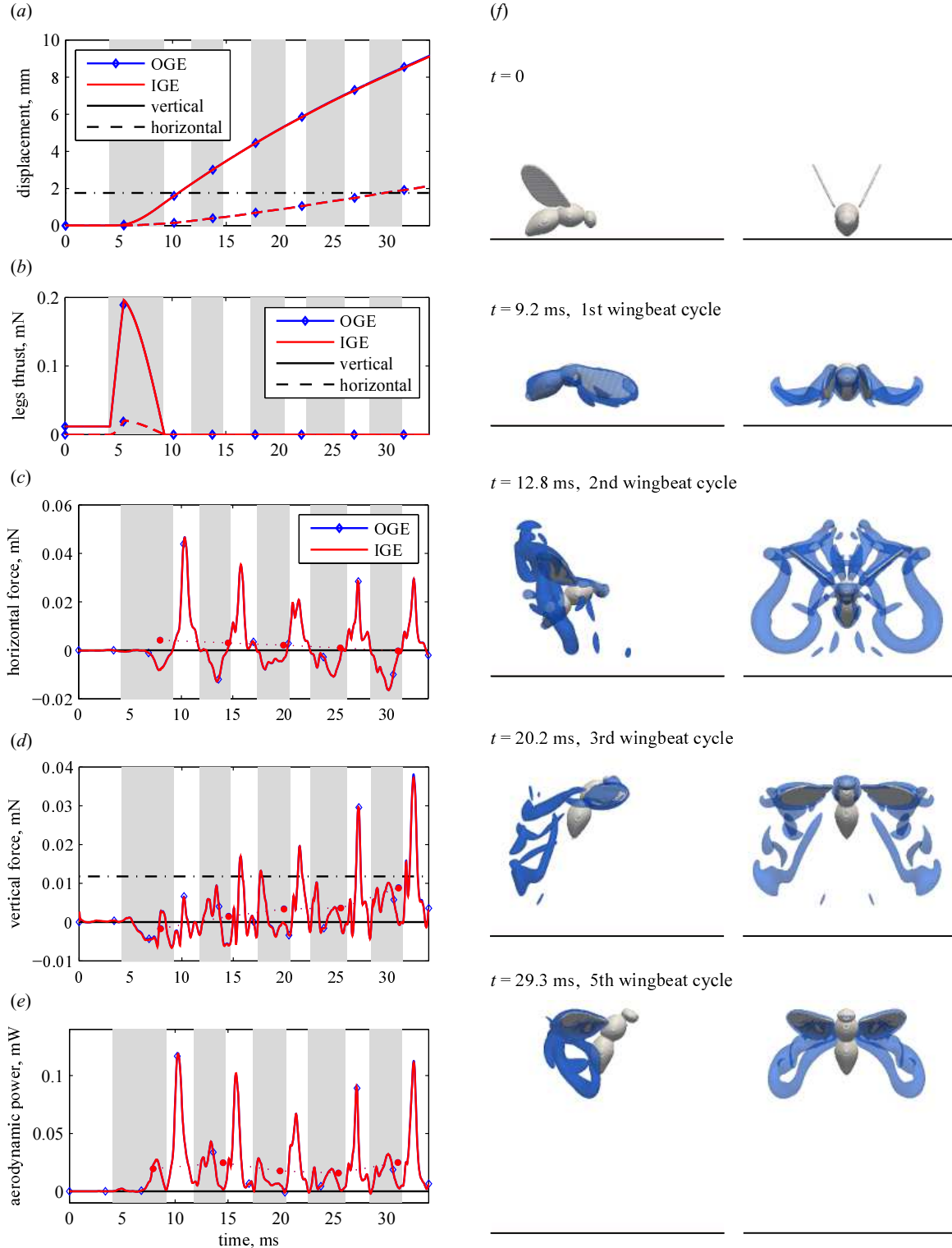


Figure 2. Voluntary takeoff. (a) Vertical and horizontal displacement. To obtain distance from the ground for the IGE case, add 1.08 mm. Dash-dotted line indicates $z_c = R$. (b) Components of the leg force. (c) vertical and (d) horizontal components of the aerodynamic force and (e) the aerodynamic power. Dash-dotted line indicates the weight. Solid circles connected by dotted lines show wingbeat cycle averages. (f) Visualization of the wings, body and ground surface, and the wake at 5 subsequent time instants, in the IGE case. Blue semi-transparent iso-surfaces show the Q -criterion.

z_c is already larger than the wing length R . Therefore, the aerodynamic interference with the ground is expected to be negligible. Note that the kinematics during the first two wingbeat cycles are a transient. After that, the time evolution of the wing angles approaches a periodic regime and the stroke plane becomes less inclined with respect to the ground. At $t = 29.3$ ms, the new vortex ring is inclined at about 45° .

The displacement of the body point of reference is shown in figure 2(a). It presents the evolution of the vertical component $\zeta(t) = z_c(t) - z_c(0)$ and the horizontal component $\xi(t) = x_c(t) - x_c(0)$ over time for the cases IGE and OGE. At the end of the 5th wingbeat cycle, $t = 34$ ms, the insect gains 9.1 mm of altitude and propels 2.1 mm forward. These numbers are consistent with the trajectories shown in [4]. The displacements IGE and OGE differ by less than 1%. Therefore, the ground effect on ζ and ξ is indeed negligible.

Figure 2(b) shows the two components of the leg force. At $t = 0$, the vertical component of the leg force is equal to the weight and the horizontal component is zero. The jump is triggered at $t_\ell = 4.2$ ms. At time $t_\ell + \tau_\ell = 5.5$ ms, both components reach their peaks. After that the force decreases and vanishes at $t = 9.3$ ms, when the legs lose contact with the ground. Note that the leg thrust can, in principle, be different for the takeoffs IGE and OGE, because the leg model depends on the aerodynamic force *via* $z_c(t)$. However, for the voluntary takeoff considered here, there is no influence of the ground effect.

The vertical and the horizontal components of the aerodynamic force are shown in figures 2(c) and (d), respectively. Over the first four wingbeat cycles, the wingbeat averaged aerodynamic forces are significantly lower than the weight. This can be explained by the large initial rate of climb due to the leg thrust, which cannot be supported by the wings. During the fifth wingbeat, the wings support 76% of the weight. The ground effect is, again, negligible. Even during the first wingbeat cycle, when the wings approach the ground surface, the difference is less than 7% of the instantaneous vertical force. The wingbeat cycle averaged forces differ by at most 2% of the weight.

Figure 2(e) displays the time evolution of the aerodynamic power, when operating IGE and OGE. Note that, in this study, we do not consider the inertial power because the wings have the same kinematics in both cases, IGE and OGE. Therefore, the inertial power is the same. The aerodynamic power is the aerodynamic component of the power required to actuate the wings,

$$P = -\mathbf{M}_l \cdot (\boldsymbol{\Omega}_l - \boldsymbol{\Omega}_b) - \mathbf{M}_r \cdot (\boldsymbol{\Omega}_r - \boldsymbol{\Omega}_b). \quad (6)$$

In (6), M_l and M_r are the aerodynamic moments of the left and of the right wing, respectively, relative to the corresponding pivot point. $\boldsymbol{\Omega}_l$ and $\boldsymbol{\Omega}_r$ are the angular velocities of the wings and $\boldsymbol{\Omega}_b$ is the angular velocity of the body. All vectors are taken in the laboratory frame of reference. P is positive if power is consumed. We find that it is positive during most part of the takeoff (see figure 2e). Only at the reversals during the first two cycles, when the body velocity is still small, P is slightly negative. During the 5th wingbeat, which produces the largest vertical force, the mean body-mass specific aerodynamic power is equal to $P_b^* = P_{ave}/m = 21$ W/kg. Assuming

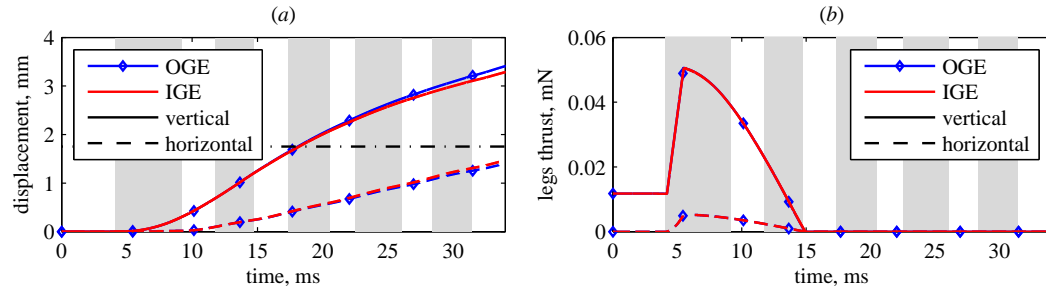


Figure 3. Slow vertical takeoff. (a) Vertical and horizontal displacement. Dash-dotted line indicates $z_c = R$. (b) Components of the leg force.

that the muscles contribute to 30% of the body mass, the mean muscle-mass specific aerodynamic power is equal to $P_m^* = P_{ave}/(0.3m) = 69$ W/kg. These estimates are close to the values reported for the hovering flight [19, 8]. The relative difference in the cycle averaged values between IGE and OGE is less than 2% during the first wingbeat cycle and less than 1% during the subsequent cycles.

We conclude that the ground effect is unimportant for the voluntary takeoff, a result which is in agreement with [4]. This is mainly a consequence of rapid acceleration during the first wingbeat cycle, when the legs produce a large vertical force. The main question of the next section is whether this scenario changes if the takeoff is slower and the insect remains near the ground for a longer time. The rate of climb at the beginning of takeoff is controlled by the leg model rate coefficient K_ℓ^+ , and the horizontal velocity is controlled by the leg angle ϕ_ℓ^+ .

3.2. Slow takeoff

This section describes a modified takeoff with the leg thrust coefficient decreased to $K_\ell^+ = 0.041$ N/m (see the second line in table 1). Smaller K_ℓ^+ results in less leg thrust and slower climb, compared to the natural voluntary takeoff. Therefore we refer to this case as a ‘slow takeoff’. In these computations, the computational domain size, the number of grid points and the penalization parameter are the same as in the previous section.

Figure 3(a) shows the displacement of the body point of reference. The rate of climb is about one third of its original value and the insect only gains 3.3 mm by the end of the 5th wingbeat cycle. This is just slightly larger than the wing length R (2.83 mm). There is a small difference between the vertical displacement in the cases IGE and OGE. Surprisingly, the ground effect reduces the rate of climb. In the horizontal direction, the displacement is larger for IGE than for OGE. The time evolution of leg thrust is given in figure 3(b). There is no visible difference between the two cases. The peak of the vertical force is equal to 0.051 mN, which is about four times less than in the original voluntary takeoff discussed in section 3.1.

The time evolution of the instantaneous aerodynamic force is qualitatively similar

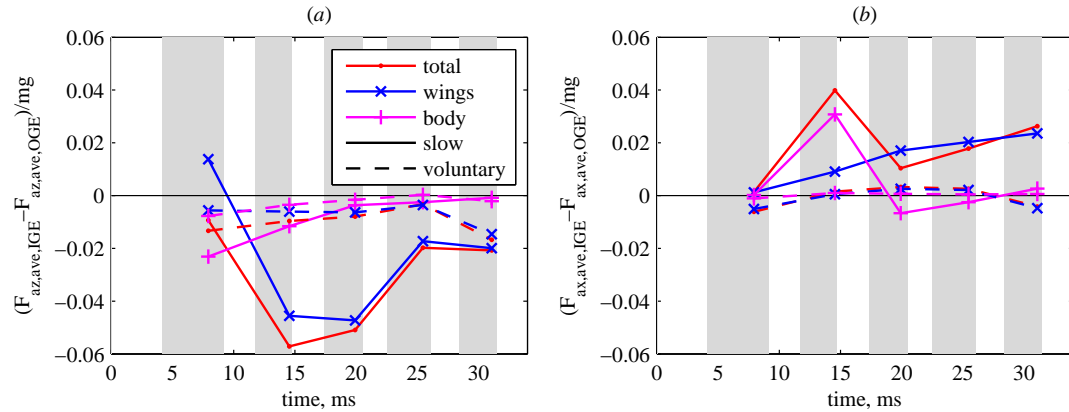


Figure 4. Slow vertical takeoff. The difference between the cases IGE and OGE, in terms of the wingbeat cycle averaged aerodynamic force normalized by the body weight (a) vertical and (b) horizontal components. The forces acting on the wings and the body are shown separately. The total force, which is their sum, is also shown.

to the voluntary takeoff case considered previously. Let us focus on the wingbeat averaged force. Figure 4 shows the difference between forces in the cases IGE and OGE, normalized by the weight. Solid lines correspond to the ‘slow’ takeoff. The ground effect decreases the total vertical force and increases the total horizontal force, with the exception of the first wingbeat. The vertical force decrease is up to 6%. It is mainly due to the decreased force of the wings. The contribution of the body in both components of the ground effect force is at most 3%, and it decays after the first two wingbeats. The natural voluntary takeoff is shown with dashed lines. The ground effect is much smaller, but the trends are similar.

The decrease of $F_{az,ave,IGE}$ during takeoff IGE contrasts to the increase of lift observed during hovering near the ground [19], which was mainly due to the body force. The difference is partly explained by the fact that the vertical force acting on the body in takeoff in ground effect is smaller than during hovering near the ground. In hovering, the lift is enhanced from the second wingbeat cycle on by means of the “air cushion” owing to the downwash produced in the previous wingbeat cycle. However, in takeoff, during the first cycle, the fluid momentum is directed essentially backwards, and during subsequent cycles the distance between the abdomen and the ground increases such that the fountain effect weakens.

Figure 5 compares the flow at $t = 18.3$ ms, in the cases OGE and IGE. There are remarkable differences. Wake vortices are distorted by the ground proximity, and some attached vortical structures appear on the ventral side of the body. Plots of the velocity vector indicate an upward flow in the gap between the body and the ground, which is the fountain effect also present during hovering [19]. However, note that the flow is essentially unsteady, therefore, visualization at a single time instant only provides some qualitative insight. Quantitative conclusions can only be drawn from time-averaged quantities such as cycle averaged forces.

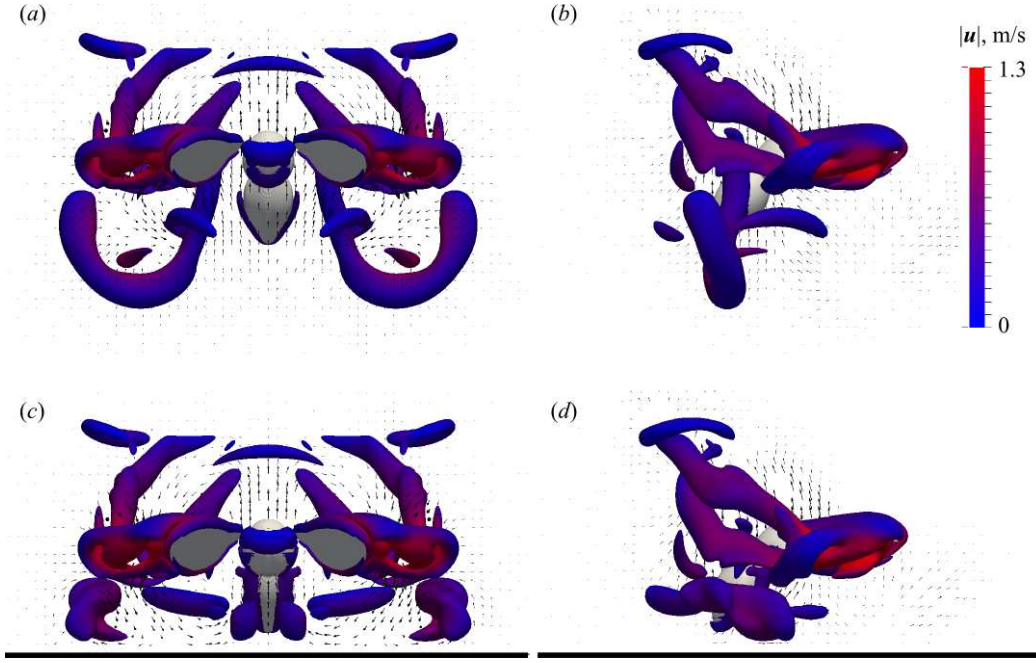


Figure 5. Slow vertical takeoff. Flow visualization at time $t = 14.7$ ms. Iso-surfaces show the Q -criterion coloured with the velocity magnitude. Vector plots show the velocity in a vertical plane that passes through the wing pivot points and in the symmetry plane. (a) OGE, front view; (b) OGE, side view; (c) IGE, front view; (d) IGE, side view. The black horizontal line indicates the ground in the IGE case.

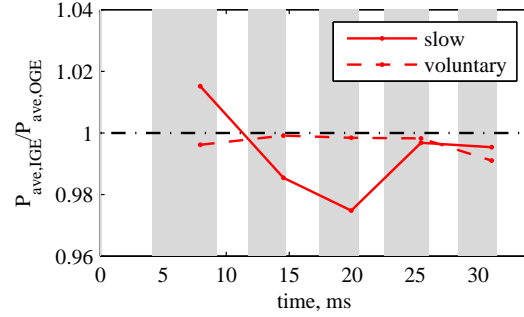


Figure 6. Aerodynamic power ratio IGE/OGE.

The aerodynamic power, in the cases IGE and OGE, is compared in figure 6. The difference is of about 2% in magnitude for the slow takeoff, but less than 1% for the voluntary takeoff. Considering the slow takeoff, the insect consumes more power when operating in ground effect (IGE) during the first wingbeat cycle, but less power during the subsequent cycles.

The negative lift force on the wings is an unexpected effect. This may be the result of complex wing-wake-ground interactions that depend on the wing and the body kinematics. Adverse ground effects have been reported previously for fixed-wing aircraft [12], but they consist in increased drag together with increased lift. However, for a

two-dimensional ellipse with normal hovering kinematics [9], the mean vertical force decreases at intermediate distances from the ground. For flapping wings, an adverse ground effect was found by Quinn et al. [20]. They considered an airfoil undergoing pitch oscillations in a closed-loop water channel with prescribed free-stream velocity. Such a configuration represents a section of a bird wing in forward flight or a fish fin. Even if the pitching motion was symmetric, the proximity of the ground broke the symmetry of the flow. Thus, the airfoil produced non-zero lift. The lift was positive if the distance to the ground was less than 40% of the chord length, but it became negative at larger distances, such that the lift force pulled the airfoil towards the ground. Note that the extra propulsive force due to the ground effect was positive in all cases.

In the present work, we find a similar effect. The wingbeat cycle averaged vertical force of the wings in the ground effect is slightly larger during the first cycle. As the insect goes away from the ground, the vertical force in the case IGE becomes less than in the case OGE. The cycle averaged horizontal force is larger at all times in the case IGE.

There is likely to be a qualitative difference between the ground effect with and without horizontal velocity. During takeoff considered in this study, the kinematics is such that the wings induce some horizontal flow, which makes it similar to horizontal flight [20]. During hovering [19], there is no adverse ground effect as the average horizontal velocity is zero. Note, however, that the flow considered in the present study is essentially three-dimensional and there are strong wing-vortex interactions present, which is not the case in [20].

3.3. Takeoffs with simplified kinematics

In the previous sections we noticed that the ground effect depends on the takeoff kinematics. We are mainly interested in the effects that might be generally applicable to a fruitfly sized insect takeoff. Therefore, in this section we consider parametric studies. They are performed using simplified periodic wing kinematics. The time evolution of the three wing angles over one wingbeat period is shown in figure 7. This takeoff mode can be relevant to MAVs, for which the wing kinematics and the body angle do not change over the wingbeats. The leg strength parameter K_l^+ is varied, resulting in a variation of the takeoff rate of climb $V_{t.o.}$. The body angle is constant and equal to $\beta = 46.3^\circ$, the anatomical stroke plane angle is equal to $\eta = 32^\circ$. In these computations, we use $L_x = L_y = 4R$, $L_z = 6R$, $N_x = N_y = 256$ and $N_z = 384$. The penalization parameter is equal to $\varepsilon = 2.5 \cdot 10^{-4}$.

Smaller K_l^+ imply smaller rate of climb (figure 8c) which leads to a more significant ground effect (figure 8d). The effect on the vertical force is, again, adverse - the force is decreased by up to 8%. The horizontal force increases slightly, 3% at most. A striking feature of figures 8(a) and (b) is that the difference between the forces IGE and OGE increases in time, even though the distance also increases. This is consistent with the hypothesis of the vortices bouncing away from the ground surface and later approaching

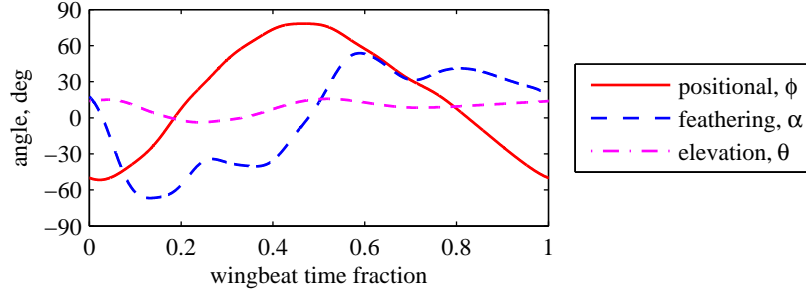


Figure 7. Wing kinematics obtained by periodization of the last wingbeat shown in [4]. In the discussion in section 3.4, this case is referred to as CS. Note that the cycle begins from the upstroke.

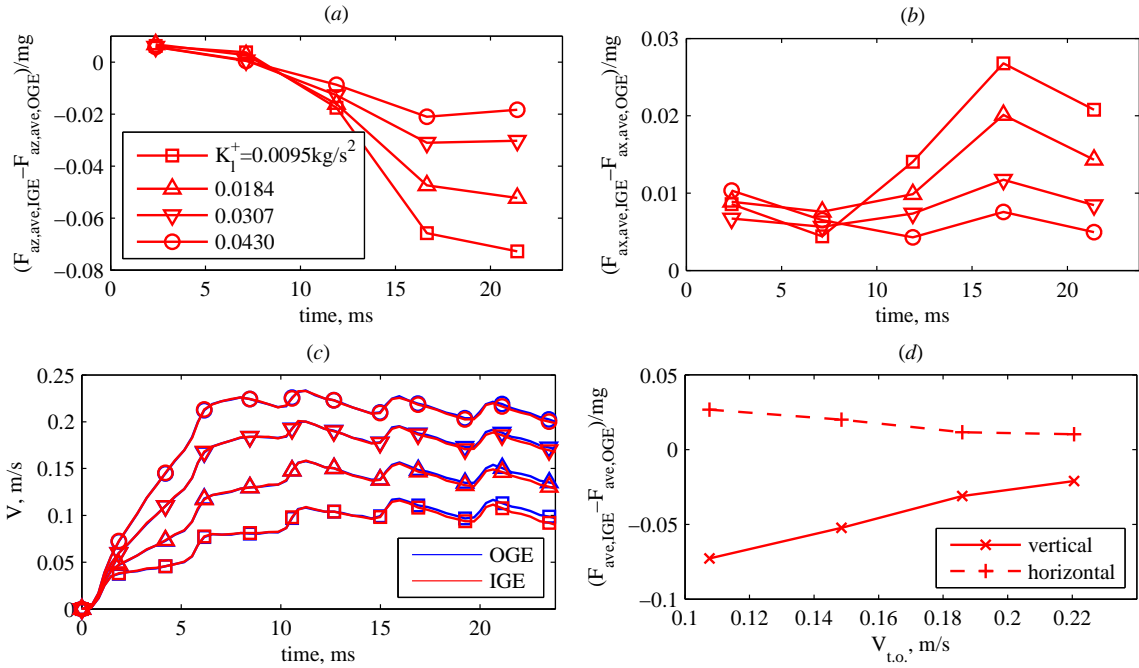


Figure 8. (a) Vertical and (b) horizontal difference between the wingbeat-averaged force IGE and OGE, normalized to the insect weight. (c) Vertical velocity of the body point of reference (rate of climb) versus time. (d) Maximum normalized force difference versus takeoff rate of climb at the moment when the legs lose contact with the ground.

the wings being the main mechanism.

3.4. Ground effect in hovering flight

In this section, we simplify the kinematics even further. We consider hovering with the insect body being fixed. The distance from the body centre to the ground is equal to $0.48R$ (where R is the wing length) for hovering in ground effect (IGE) and $2.4R$ for hovering out of ground effect (OGE). The body pitch angle and the anatomical stroke

plane angle are both constant and equal to 55° , such that the stroke plane is horizontal. The wing kinematics is the same as in the previous section, see figure 7. We denote it as ‘CS’ kinematics. The first wingbeat starts from the upstroke, as done in [4].

In these numerical simulations we are interested in the long-time evolution of the aerodynamic forces, which after the initial transient eventually reach a periodic state. Most of the results known from the helicopter rotor theory [16] are obtained in reference to the periodic state, while the takeoffs considered in the previous sections of this paper (the slow takeoffs, in particular) last only for a few wingbeats. Therefore, it is instructive to consider the time evolution of the aerodynamic forces during hovering from $t = 0$ until the time when the periodic state is reached.

Since the time span of the numerical simulations presented in this section is large, it is necessary to increase the domain size in the horizontal directions. We set $L_x \times L_y \times L_z = 8R \times 8R \times 4R$, where z is the vertical direction. The number of grid points is $N_x \times N_y \times N_z = 864 \times 864 \times 432$. The penalization parameter is equal to $\varepsilon = 2.5 \cdot 10^{-4}$.

The quantity of interest is the ratio of the wingbeat averaged forces, IGE to OGE: $F_{z,ave,IGE}/F_{z,ave,OGE}$. This quantity is shown in figure 9(a). The red solid line with “+” symbols corresponds to the total vertical force ratio. As already noticed in [19], the vertical force during hovering in ground effect, $F_{z,IGE}$, reaches its periodic state significantly later than during hovering out of ground effect, $F_{z,OGE}$. Therefore, the ratio of their wingbeat averages, $F_{z,ave,IGE}/F_{z,ave,OGE}$ converges slowly with the number of wingbeats. It oscillates between 102% and 107%. After 27 wingbeats it reaches 106%.

A similar comparison for the force generated by the wings is shown with a red dashed line. It was calculated by integration of the distributed forces over the wings only, in the same numerical simulations. Therefore, the aerodynamic interaction between the body and the wings is included. This force ratio drops from 100.6% to 92.5% during the first 6 wingbeats, oscillates and then increases to 96.3%. The initial time evolution of the vertical force ratio of the wings, over the first three or four cycles, is qualitatively similar in all cases. It takes place before the vortex wake ‘rebounds’ from the ground surface. After that, the oscillation of the vertical force IGE can be attributed to the wing-wake interaction, which is sensitive to the wing kinematics. We discuss different wing kinematics later in this section.

The time evolution of the wake vortices generated by the insect is shown in figure 10. The visualized time instants correspond to the end of the 1st, 2nd, ..., 25th downstroke. There are significant differences between the positions of the vortices over the first four time instants. The first wingbeat generates very strong vortex rings, that collide with the ground. Then they rebound during the second wingbeat, and parts of them moving upwards are still visible during the third wingbeat. The downwash produced by these vortices influences the nearer wake dynamics and it is likely to be responsible for the decrease of the vertical force during the first few wingbeats. After the 10th wingbeat, the wake approaches its quasi-periodic state. There are almost no visible differences between the visualizations at the end of the 20th wingbeat and at the end of the 25th

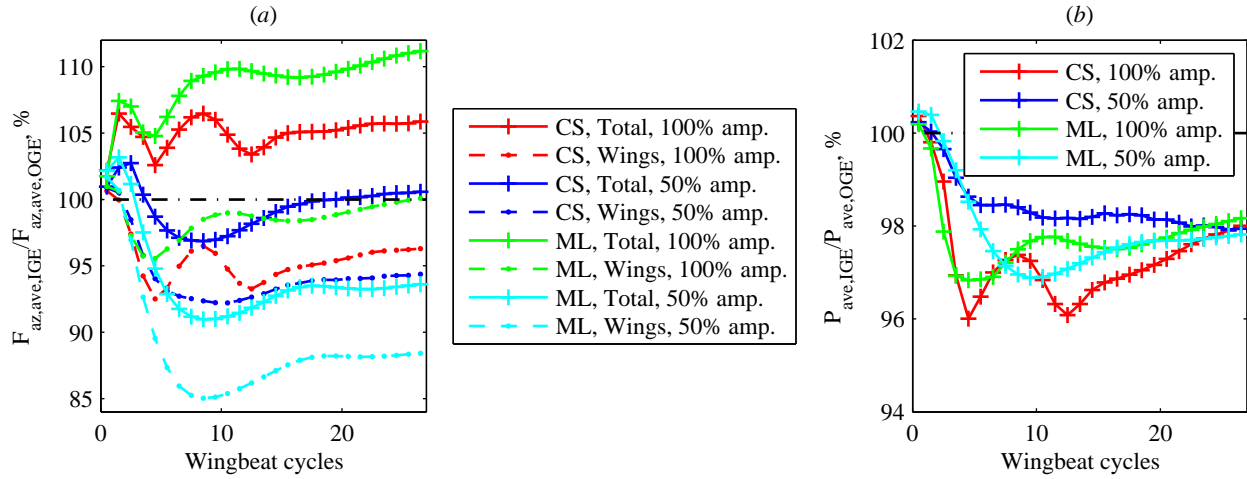


Figure 9. (a) The ratio of wingbeat averaged vertical force IGE to OGE, $F_{z,ave,IGE}/F_{z,ave,OGE}$. (b) The ratio of wingbeat averaged power IGE to OGE, $P_{ave,IGE}/P_{ave,OGE}$.

wingbeat.

The pair of numerical simulations (cases IGE and OGE) that we have discussed in the above paragraphs leads to the following conclusions.

- (i) Over the first 27 wingbeats, $F_{z,ave,IGE}/F_{z,ave,OGE}$ varies within about 5% for the total force and 9% for the wings force.
- (ii) The wing generates less vertical force in the case IGE than in the case OGE (adverse ground effect).
- (iii) The body makes an important contribution to the total vertical force when operating IGE, which results in the excess total vertical force (positive ground effect).

These conclusions are, of course, only valid for the particular wing shape and kinematics used in the simulation. Periodic flapping is only an approximation to the real insect wing motion, which varies from one wingbeat to another, and depends on many different conditions. To determine the effect of all existing fruitfly wing kinematics is beyond the reach of our numerical simulations. However, it is useful to compare a few different cases.

We carried out numerical simulations with the wing kinematics used in [19] (abbreviated as ‘ML’ in the figures). Note that, in this case, the first wingbeat begins from the downstroke. The results of these numerical simulations are shown in figure 9 with green lines. They are qualitatively similar to the previously shown ‘CS’ case, but the values are systematically larger. $F_{z,ave,IGE}/F_{z,ave,OGE}$ reaches 111% for the total force and 100% for the wings, such that there is no adverse ground effect after the periodic state is established.

The adverse ground effect is rarely encountered in the aircraft or rotorcraft

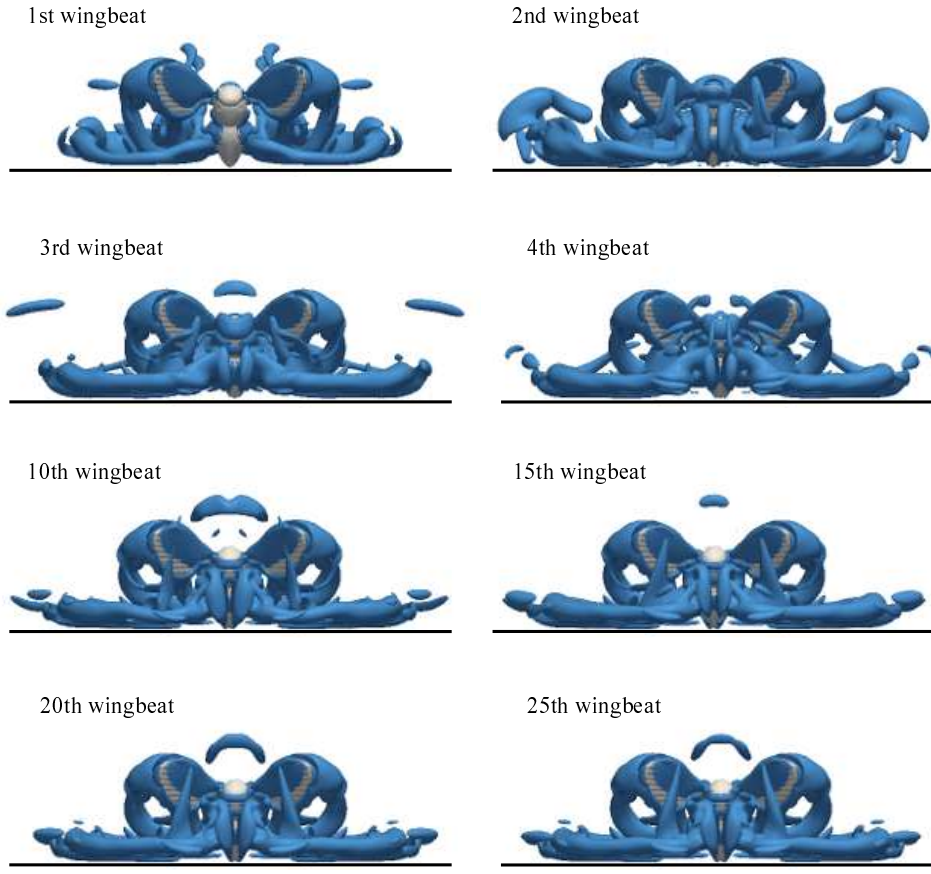


Figure 10. Time evolution of the wake. Isosurfaces of the Q -criterion are shown at the end of the downstroke. ‘CS’ kinematics with 100% wingbeat amplitude.

aerodynamics literature. However, in the context of flapping wings, it is not unusual. In the two-dimensional numerical simulations [9], a U-shape profile of the force ratio $F_{z,ave,IGE}/F_{z,ave,OGE}$ versus h/c was found, where h is the distance from the wing centre to the ground and c is the wing chord. $F_{z,ave,IGE}/F_{z,ave,OGE}$ was greater than 100% for $h/c < 1.5$, but less than 100% for $h/c > 1.5$, and the minimum ratio was of about 54%.

In the three-dimensional model considered in the present paper, it is possible to partially reduce the three-dimensional effects by decreasing the wing beat amplitude. One can then expect the adverse ground effect to be amplified. Indeed, this is what we find by decreasing the wingbeat amplitude by a factor of 2 (by rescaling the positional angle shown in figure 7 such that the amplitude is halved and the mean value is unchanged). The results are shown in figure 9 with blue lines. Now we have $F_{z,ave,IGE}/F_{z,ave,OGE} < 100\%$ at intermediate times, for wings force and for the total force. The final periodic state produces a very slight excess of the total vertical force (less than 1%). Note that, in this reduced-amplitude case, the total force ratio decreases more than the wing force ratio. This indicates, not surprisingly, that the fountain effect becomes weaker when the wingbeat amplitude is reduced. Similar

computations with the ‘ML’ kinematics show the same trend with an even larger decrease of $F_{z,ave,IGE}/F_{z,ave,OGE}$.

The wingbeat averaged aerodynamic power ratio $P_{ave,IGE}/P_{ave,OGE}$ is shown in figure 9(b). Its variation is smaller than the variation of the force, and the computations suggest that its long-time limit is between 97% and 99%, in all cases that we have considered. The shape of the time evolution profiles of the power ratio is approximately similar to the time profiles of the wings vertical force ratio. This means that a local decrease of the vertical force ratio is accompanied by a decrease of the power ratio. Therefore, if the kinematics of the wings operating in ground effect is adjusted such that $P_{ave,IGE}/P_{ave,OGE} = 100\%$ at any time, the force ratio $F_{z,ave,IGE}/F_{z,ave,OGE}$ is likely to increase. Among other factors, the feathering angle is very likely to change passively, when in ground effect, due to compliance of the wing [10, 23, 11]. Such effects would need further investigation.

4. Conclusions

Numerical simulations of insect takeoff have been carried out. The three-dimensional incompressible Navier–Stokes equations were solved using a pseudo-spectral method with volume penalization [15, 14], in order to obtain the flow field and the aerodynamic forces acting on the insect. The takeoff trajectories were calculated using a simple flight dynamics solver that accounts for the body weight, inertia, and the legs thrust. A series of computations has been carried out to explore the parametric space of the model. A natural voluntary takeoff of a fruitfly, modified takeoffs and hovering flights have been compared.

We found that the ground effect during the natural voluntary takeoff is negligible. The wingbeat averaged forces only differ by less than 2% of the weight. The aerodynamic power also differs by less than 2%.

In the modified takeoffs, we decreased the leg strength. As a consequence, the rate of climb decreased and the ground effect became significant. In most cases, the vertical force decreased (by 8% of the weight at most), evidently due to the downwash from the vortex rings that rebounded from the ground surface. The horizontal force slightly increased (up to 4% of the weight).

During hovering near the flat ground surface, the fountain effect produces a large upward force on the insect’s body. The net ground effect is therefore positive. However, the aerodynamic force acting on the wings in ground effect is often less than when the wings operate out of ground effect. The most significant decrease is during the first 15 wingbeats. Note that this is a much longer time period than a typical takeoff. At long time hovering, the effect may be positive or negative, depending on the wings kinematics. The power in ground effect slightly decreases in all cases, by 4% at most and by about 2% in the long time limit.

To summarize, the main conclusion is that, during fruitfly sized insect or MAV takeoff in ground effect, the vertical force does not increase. Moreover, it even drops

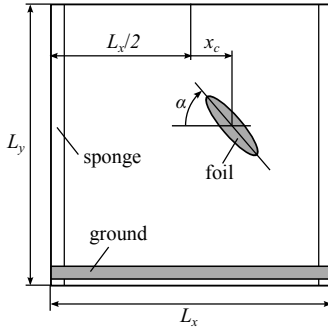


Figure A1. Schematic drawing of the setup.

in most of the cases that we considered. There is, however, a consistent increase of the horizontal force, and a decrease of the aerodynamic power, if the rate of climb is sufficiently small.

Acknowledgments

Numerical simulations were carried out using HPC resources of IDRIS, Paris (project 81664) and of Aix-Marseille Université (project Equip@Meso). DK gratefully acknowledges the financial support from the CRM-ISM Postdoctoral Fellowship. TE and KS thank the Deutsch-Französische Hochschule / Université Franco-Allemande (DFH-UFA) for financial support.

Appendix A. Numerical validation

A numerical study of the ground effect during hovering flight was carried out by Gao and Lu [9] in the two-dimensional approximation. In this section, we compare with some of their results.

All quantities in [9] are presented in a non-dimensional form, and we follow the same conventions. The wing cross-section is an ellipse, as schematically shown in figure A1. Its major axis (chord length) is $c = 1$, and its minor axis is equal to 0.25. The motion of the ellipse centre in the horizontal direction (x direction) is given by

$$x_c(t) = A_m \cos(2\pi t/T), \quad (\text{A.1})$$

where $A_m = 1.25$, and we fix the dimensionless stroke time period to $T = 2\pi A_m$. The vertical coordinate of the ellipse centre is constant in time. The angle between the major axis and the horizontal axis varies according to

$$\alpha(t) = \alpha_0 - \alpha_m \sin(2\pi t/T), \quad (\text{A.2})$$

where $\alpha_0 = 90^\circ$ and $\alpha_m = 45^\circ$.

The ground surface is horizontal (x direction), so that the distance D between the ellipse centre and the ground remains constant in time. In the present study, we vary this parameter between 1 and 6.

The dimensionless density of the fluid is $\rho = 1$. The dimensionless kinematic viscosity is equal to $\nu = 10^{-2}$ yielding the Reynolds number

$$Re = \frac{(2\pi A_m/T)c}{\nu} = 100. \quad (\text{A.3})$$

Our method solves the three-dimensional incompressible Navier–Stokes equations. The two-dimensional flow is therefore modelled by imposing the initial and boundary conditions constant in the direction perpendicular to the flow plane (z direction). The domain size in this direction is $L_z = 1$.

In the xy plane, the computational domain size is equal to $L_x \times L_y = 12 \times 12$. The number of grid points is equal to $N_x \times N_y = 512 \times 512$ (*low resolution*) or 1024×1024 (*high resolution*). In the low resolution simulations, the grid step size $\Delta x \approx 0.0234$ is comparable to the lowest value reported in [9] ($\Delta x = 0.025$).

The ground is modelled as a solid layer of width 0.2. Its top surface is at distance D below the centre of the ellipse. Smoothing of the penalization mask function (erf, $3\Delta x$ inwards and $3\Delta x$ outwards, see [7]) is only applied to the ellipse, not to the ground.

The penalization parameter, both for the ellipse and for the ground, is equal to $\varepsilon = 10^{-3}$ in the low-resolution simulations and $2.5 \cdot 10^{-4}$ in the high-resolution simulations. A ‘vorticity sponge’ forcing term [7] is introduced in the momentum equation equation in order to weaken the effect of the periodic boundary conditions in x . It is applied in two vertical layers of thickness equal to $32\Delta x$, and its penalization parameter is equal to $\varepsilon_{\text{sponge}} = 0.1$.

The nearest distance to the ground in [9] is $D = 1$. Figure A2(a) displays the time evolution of the vertical force coefficient C_V , obtained by normalizing the vertical force F_V ,

$$C_V = \frac{F_V}{0.5\rho U^2 c L_z}. \quad (\text{A.4})$$

where $U = 2\pi A_m/T$. In the figures, the time t is normalized to the stroke period T . After $t/T = 1$, oscillations of C_V are mainly described by the second harmonic. They become apparently periodic after $t/T = 4$.

A series of simulations has been carried out in order to determine how the time averaged force coefficients depend on D . Their parameters correspond to the low resolution, as defined above. As shown in figure A2(b), the minimum of C_V is observed in our simulations at about the same D as in [9]. We conclude that, in this two-dimensional validation case, our results are in reasonable agreement with the reference [9].

- [1] P. Angot, C.-H. Bruneau, and P. Fabrie. A penalisation method to take into account obstacles in viscous flows. *Numer. Math.*, 81:497–520, 1999.
- [2] G. Bimbard, D. Kolomenskiy, O. Bouteleux, J. Casas, and R. Godoy-Diana. Force balance in the take-off of a pierid butterfly: relative importance and timing of leg impulsion and aerodynamic forces. *Journal of Experimental Biology*, 216(18):3551–3563, 2013.
- [3] G. Card and M. Dickinson. Performance trade-offs in the flight initiation of *Drosophila*. *Journal of Experimental Biology*, 211(3):341–353, 2008.

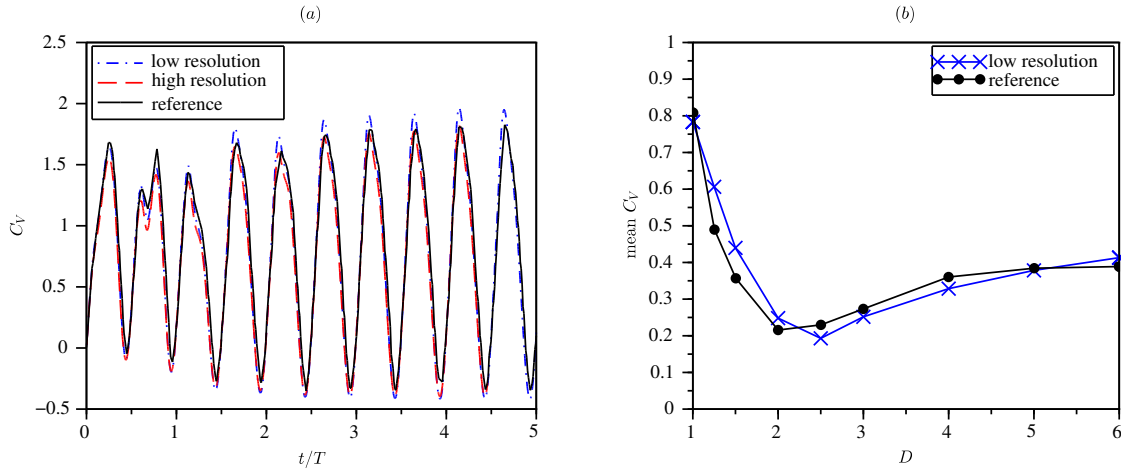


Figure A2. (a) Time evolution of the vertical force coefficient C_V at the distance from the ground $D = 1$. (b) Mean vertical force coefficient versus distance from the ground.

- [4] M. W. Chen and M. Sun. Wing/body kinematics measurement and force and moment analyses of the takeoff flight of fruitflies. *Acta Mechanica Sinica*, 30(4):495–506, 2014.
- [5] M. W. Chen, Y. L. Zhang, and M. Sun. Wing and body motion and aerodynamic and leg forces during take-off in droneflies. *Journal of The Royal Society Interface*, 10(89), 2013.
- [6] M. H. Dickinson, F.-O. Lehmann, and S. P. Sane. Wing rotation and the aerodynamic basis of insect flight. *Science*, 284:1954–1960, 1999.
- [7] T. Engels, D. Kolomenskiy, K. Schneider, and J. Sesterhenn. Numerical simulation of fluid-structure interaction with the volume penalization method. *Journal of Computational Physics*, 281:96–115, 2015.
- [8] S. N. Fry, R. Sayaman, and M. H. Dickinson. The aerodynamics of hovering flight in *Drosophila*. *Journal of Experimental Biology*, 208(12):2303–2318, 2005.
- [9] T. Gao and X. Lu. Insect normal hovering flight in ground effect. *Physics of Fluids*, 20:087101, 2008.
- [10] D. Ishihara, T. Horie, and M. Denda. A two-dimensional computational study on the fluidstructure interaction cause of wing pitch changes in dipteran flapping flight. *Journal of Experimental Biology*, 212(1):1–10, 2009.
- [11] D. Ishihara, T. Horie, and T. Niho. An experimental and three-dimensional computational study on the aerodynamic contribution to the passive pitching motion of flapping wings in hovering flies. *Bioinspiration & Biomimetics*, 9(4):046009, 2014.
- [12] B. L. Jones. *Experimentant investigation into the aerodynamic ground effect of a tailless chevron-shaped UCAV*. PhD thesis, Department of the Air Force, Air University, Air Force Institute of Technology, Wright-Patterson Air Force Base, Ohio, USA, 2005.
- [13] E. J. Kim, M. Wolf, V. M. Ortega-Jimenez, S. H. Cheng, and R. Dudley. Hovering performance of Anna's hummingbirds (*Calypte anna*) in ground effect. *Journal of The Royal Society Interface*, 11(98):20140505, 2014.
- [14] D. Kolomenskiy, H. K. Moffatt, M. Farge, and K. Schneider. Two- and three-dimensional numerical simulations of the clap–fling–sweep of hovering insects. *J. Fluids Struct.*, 27(5-6):784–791, 2011.
- [15] D. Kolomenskiy and K. Schneider. A Fourier spectral method for the Navier–Stokes equations with volume penalization for moving solid obstacles. *Journal of Computational Physics*, 228:5687–5709, 2009.
- [16] J. G. Leishman. *Principles of helicopter aerodynamics*. Cambridge University Press, 2006.

- [17] Y. Liu, N. Liu, and X. Lu. Numerical study of two-winged insect hovering flight. *Advances in Applied Mathematics and Mechanics*, 1(4):481–509, 2009.
- [18] M. Maeda. *Aerodynamics of flapping flight interacting with environments*. PhD thesis, Biomechanical Engineering Laboratory, Graduate School of Engineering, Chiba University, 2014.
- [19] M. Maeda and H. Liu. Ground effect in fruit fly hovering: A three-dimensional computational study. *Journal of Biomechanical Science and Engineering*, 8(4):344–355, 2013.
- [20] D. B. Quinn, K. W. Moored, P. A. Dewey, and A. J. Smits. Unsteady propulsion near a solid boundary. *Journal of Fluid Mechanics*, 742:152–170, 3 2014.
- [21] J. M. V. Rayner. On the aerodynamics of animal flight in ground effect. *Philosophical Transactions of the Royal Society of London. Series B: Biological Sciences*, 334(1269):119–128, 1991.
- [22] K. Schneider. Numerical simulation of the transient flow behaviour in chemical reactors using a penalisation method. *Computers & Fluids*, 34:1223–1238, 2005.
- [23] H. Tanaka, J. P. Whitney, and R. J. Wood. Effect of flexural and torsional wing flexibility on lift generation in hoverfly flight. *Integrative and Comparative Biology*, 51(1):142–150, 2011.
- [24] Y. Tanida. Ground effect in flight. *JSME International Journal Series B*, 44(4):481–486, 2001.
- [25] T. V. Truong, D. Byun, M. J. Kim, K. J. Yoon, and H. C. Park. Aerodynamic forces and flow structures of the leading edge vortex on a flapping wing considering ground effect. *Bioinspiration & Biomimetics*, 8(3):036007, 2013.
- [26] J. Wu, C. Shu, N. Zhao, and W. Yan. Fluid dynamics of flapping insect wing in ground effect. *Journal of Bionic Engineering*, 11:52–60, 2014.
- [27] N. Zumstein, O. Forman, U. Nongthomba, J. C. Sparrow, and C. J. H. Elliott. Distance and force production during jumping in wild-type and mutant *Drosophila melanogaster*. *Journal of Experimental Biology*, 207(20):3515–3522, 2004.